Supplementary Material

Atomically dispersed rhodium on ordered macroporous In_2O_3 for highly sensitive detection of ethanol and the sensing mechanism

Fubo Gu, Lanlan Zhang, Song Hong, Dongmei Han, and Zhihua Wang*

State Key Laboratory of Chemical Resource Engineering, Beijing University of Chemical Technology, Beijing 100029, China

*Corresponding author: **Zhihua Wang**

E-mail address: zhwang@mail.buct.edu.cn

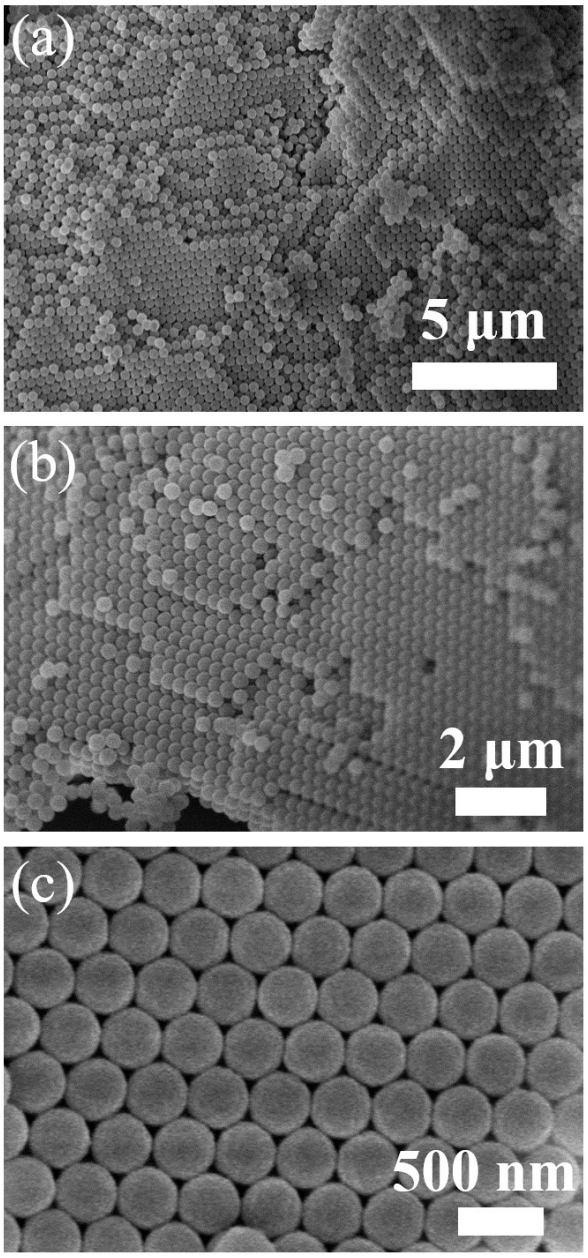

Fig. S1 SEM images of the PMMA template.

Characterization

All the samples used for the characterization were treated under H_2/Ar mixed atmosphere at 100°C (1°C/min) for 2 h. The crystal structure of the samples was investigated by X-ray diffractometer (Bruker-D8 ADVANCE) with Cu Kα1 radiation (λ=0.154056 nm) in the diffraction angle range of 5~90° at 10°/min, and the Raman spectrometer (LabRAM Aramis) in the range of 200-800 nm. The actual content of the loaded Rh was tested by inductively coupled plasma emission spectrometer (ICAP6300). The optical properties of the samples were tested by UV-visible diffuse reflectance spectroscopy (UV-2501PC) in the range of 200-800 nm. The morphology, specific surface area, and pore information were analyzed by SEM (Supra 55), four-station fully automated specific surface and pore size analyzer (BET, Quandasorb SI), and HRTEM (JEOL JEM-F200). In addition, the dispersion state of Rh was analyzed by ac-HAADF-STEM (JEOL JEM-ARM200F), CO-DRIFTS (TENSOR II) and XAFS (BL14W at the Shanghai Synchrotron Radiation Facility). The surface properties were analyzed by XPS (Axis Supra). The electrical properties of the samples were investigated by Hall effect test (RH2030). The ethanol-sensing mechanism of the sensors was investigated by the in-situ Ethanol-DRIFTS (TENSOR II) technique.[1,2] First, the samples were set in the DRIFTS cell and purged with Ar for 1 h at 260°C (the working temperature of the sensors). Then, the samples were treated with the Air for 1 h. Finally, 100 ppm ethanol (in Ar) was introduced and the DRIFTS signals were collected.

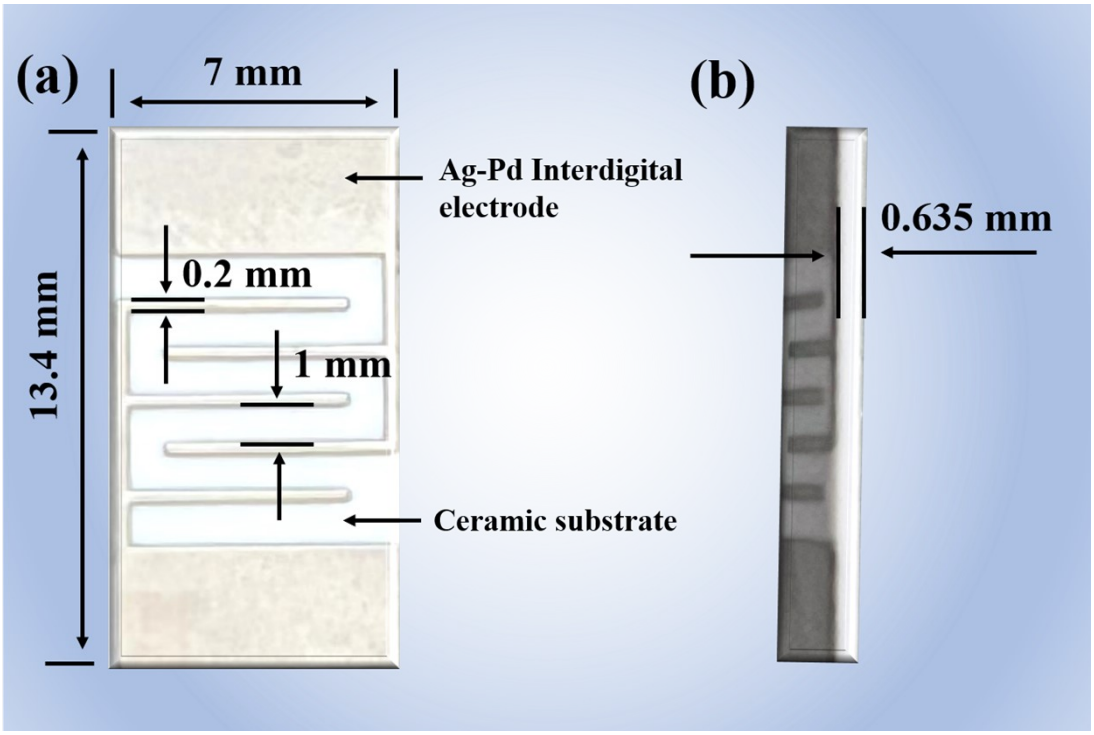

Fig. S2 The structure of Ag-Pd electrode.

The Ag-Pd electrode (Type VI) from Beijing Elite Technology Co., Ltd. with dimensions of 13.4 mm×7 mm×0.635 mm, a line width of 0.2 mm and a pitch of 1 mm.

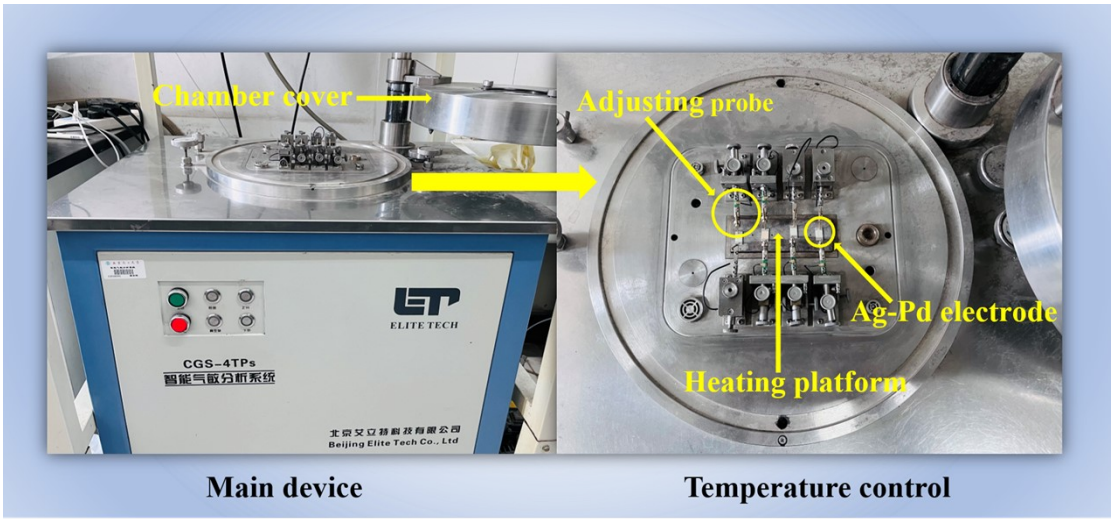

Fig. S3 Illustration of the CGS-4TPs intelligent gas sensing instrument (Beijing Elite Tech Co., Ltd).

Preparation procedure and conditions of all sample gases

The sensing tests were carried out on the CGS-4TPs intelligent gas-sensitive analysis system (Beijing Elite Tech Co., Ltd). Different concentrations of gases are obtained by a static volumetric method.[3-5] A certain amount of liquid of ethanol, acetone, propanol, methanol, methylamine, ammonia, formaldehyde and xylene were injected into the gas chamber under a relative humidity of 15 ± 5%. The liquid volume and corresponding gas concentration are calculated by eqn (1)

$$V_{liquid} = \frac{V_s C_{gas} M}{22.4 \rho d} \times 10^{-9} \quad (1)$$

Where V_{liquid} is the liquid volume, V_s is the volume of the test chamber (1.8 L) and C_{gas} is the concentration of gas. 22.4 is the gas molar volume. M, ρ and d is the molecular weight, density, and purity of the liquid. The injected volume (V_{gas}) of NO_2 gas was calculated according to eqn (2),

$$V_{gas} = V_s \times C_{gas}/C_i \quad (2)$$

Where V_s represents the volume of the test chamber, C_{gas} and C_i represent the test concentration and the initial concentration of NO_2.

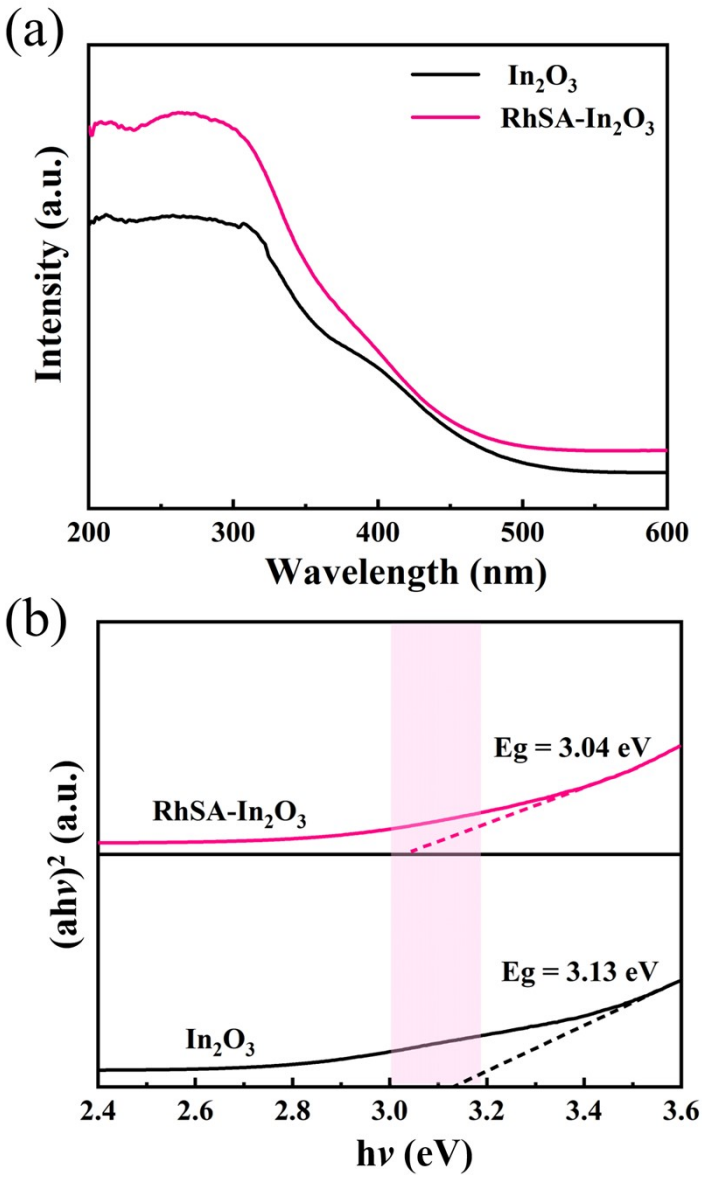

Fig. S4 (a) UV-Vis DRS spectra, (b) *(ahv)*^{2} ~ *hv* curves of In_2O_3 and RhSA-In_2O_3.

The *Eg* of the sample was calculated by Tauc eqn (3).

$$(ahv)^2 = A(hv - Eg) \quad (3)$$

where *a* is the absorption coefficient, *hv* is the photon energy, *A* is a constant related to the material, and *Eg* is the band gap energy.[6]

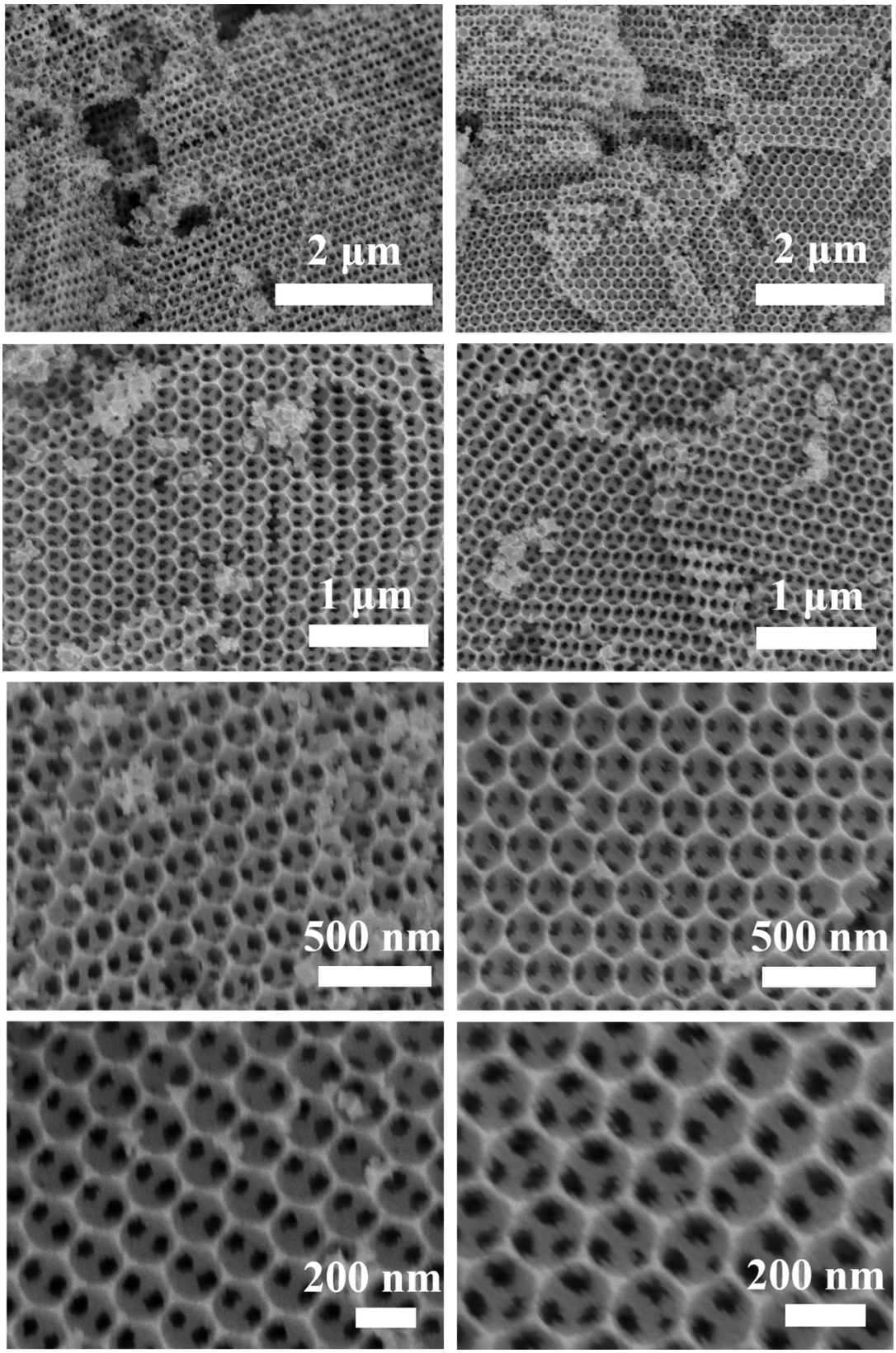

Fig. S5 SEM images of In_2O_3 (left column) and RhSA-In_2O_3 (right column) at different magnifications.

Table S1 Quantitative analyses of Rh-O and Rh-Rh contributions as measured by EXAFS.

Sample	Shell	*CN* [a]	*R*(Å)[b]	σ^2(Å^2)[c]	ΔE_0(eV)[d]	*R* factor
Rh foil	Rh-Rh	12	2.67	0.003	-6.7	0.0043
Rh_2O_3	Rh-O	6	2.04	0.004	-2.9	0.0085
RhSA-In_2O_3	Rh-O	4.5	2.05	0.001	0.3	0.0184

[a]*CN*, coordination number; [b]*R*, distance between absorber and backscatter atoms; [c]σ^2, Debye-Waller factor to account for both thermal and structural disorders; [d]ΔE_0, inner potential correction; *R* factor indicates the goodness of the fit.

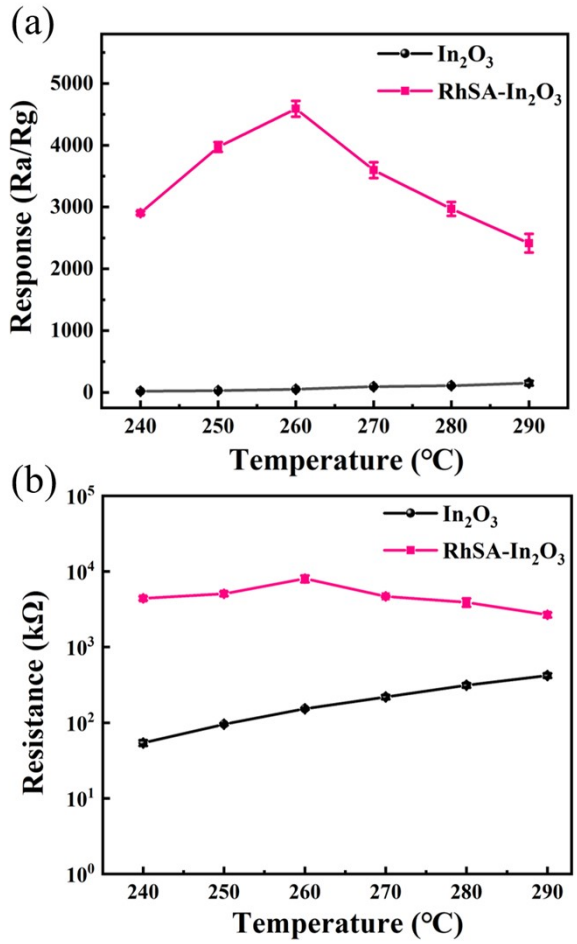

Fig. S6 Temperature-response curves to 50 ppm ethanol (a), Temperature-resistance curves (b) of the In_2O_3 and RhSA-In_2O_3 sensors.

Fig. S6(a) shows that the response of In_2O_3 is increased with the operating temperature, while RhSA-In_2O_3 has an optimum operating temperature of 260°C. The loading of atomically dispersed Rh significantly improves the ethanol-sensing response. Fig. S6(b) shows that with the increase of the operating temperature, the resistance of the sensors do not change obviously. The loading of atomically dispersed Rh increases the resistance and the reasons are as follows: when RhSA-In_2O_3 is exposed to air, the O_2 molecules in the air will be adsorbed on its surface and capture the free electrons from the conduction band of In_2O_3 to form adsorbed oxygen (O^-), which will lead to the formation of the electron depletion layer, increasing of the sensor resistance. Rh atom can act as an active site for O_2 activation and produce abundant adsorbed oxygen, which results in the high resistance of the RhSA-In_2O_3 sensor.

Calculation of the detection limit (LOD) of the sensors

The noise reflects the fluctuating level of the background signal of the instrument and can be calculated from the root mean square (*RMS*) deviation at the baseline.[7] The International Union of Pure and Applied Chemistry (IUPAC) specifies that the theoretical LOD of the sensor can be derived when the detection signal in the system is three times higher than the noise level of the instrument. Therefore, in this work, the theoretical LOD was calculated using the sensitivity (*S*) and noise level of the sensor. The calculation process is as follows: the baseline is fitted with a 5th-order polynomial (as shown in Fig. S7, each sample was tested three times), and then 11 points *Yi* are taken on the baseline, and the corresponding points *Y* on the 5th-order fitted line is calculated. After that, the residuals of the 5th-order polynomial (*Yi*-*Y*) and the corresponding *RMS* deviation are calculated. Finally, the theoretical LOD of the sensor can be calculated based on *RMS* and *S*. The calculated data are shown in Tables S2 and S3.[8-10]

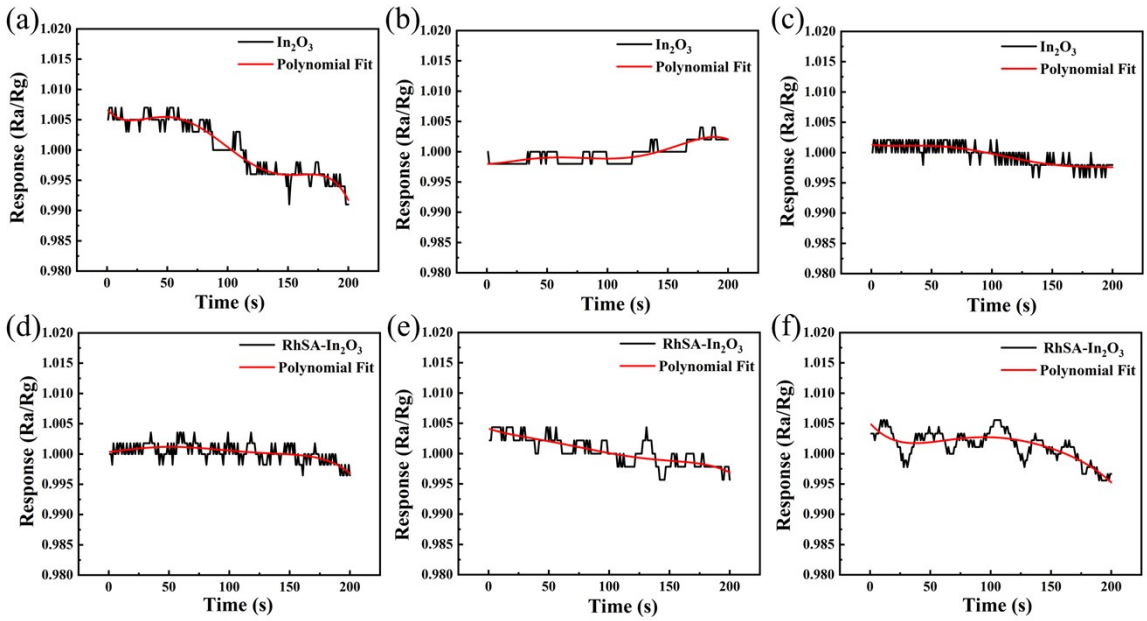

Fig. S7 Baseline curves and 5th order polynomial fit curves (red) for the In_2O_3 and RhSA-In_2O_3 sensors.

Table S2 5th order polynomial fit and theoretical detection limit data for the In_2O_3 sensor.

Time [s]	1		2		3	
	Yi-Y	$(Yi-Y)^2$	Yi-Y	$(Yi-Y)^2$	Yi-Y	$(Yi-Y)^2$
1	-1.53×10^{-3}	2.35×10^{-6}	2.01×10^{-3}	4.02×10^{-6}	-1.29×10^{-3}	1.67×10^{-6}
20	1.01×10^{-4}	1.02×10^{-8}	-3.82×10^{-4}	1.46×10^{-7}	-1.11×10^{-3}	1.24×10^{-6}
40	-3.71×10^{-4}	1.38×10^{-7}	1.13×10^{-3}	1.27×10^{-6}	-1.14×10^{-3}	1.30×10^{-6}
60	-1.46×10^{-4}	2.15×10^{-8}	-1.06×10^{-3}	1.12×10^{-6}	1.08×10^{-3}	1.17×10^{-6}
80	1.66×10^{-3}	2.75×10^{-6}	1.04×10^{-3}	1.07×10^{-6}	-5.27×10^{-4}	2.77×10^{-7}
100	-4.77×10^{-4}	2.27×10^{-7}	-8.62×10^{-4}	7.42×10^{-7}	1.98×10^{-4}	3.91×10^{-8}
120	-1.71×10^{-3}	2.94×10^{-6}	-1.09×10^{-3}	1.19×10^{-6}	1.02×10^{-3}	1.03×10^{-6}
140	1.88×10^{-3}	3.54×10^{-6}	2.13×10^{-3}	4.52×10^{-6}	-3.38×10^{-4}	1.14×10^{-7}
160	2.10×10^{-3}	4.39×10^{-6}	-1.12×10^{-3}	1.26×10^{-6}	1.15×10^{-4}	1.33×10^{-8}
180	3.13×10^{-4}	9.81×10^{-8}	-2.62×10^{-3}	6.86×10^{-8}	2.87×10^{-4}	8.23×10^{-8}
200	-7.31×10^{-4}	5.34×10^{-7}	-4.07×10^{-3}	1.66×10^{-9}	3.63×10^{-4}	1.32×10^{-7}
V_x^2	1.70×10^{-5}		1.54×10^{-5}		7.07×10^{-6}	
RMS	1.30×10^{-3}		1.24×10^{-3}		0.84×10^{-3}	
LOD (ppb)	3.52		3.36		2.27	

Table S3 5th order polynomial fit and theoretical detection limit data for the RhSA-In_2O_3 sensor.

Time [s]	1		2		3	
	Yi-Y	$(Yi-Y)^2$	Yi-Y	$(Yi-Y)^2$	Yi-Y	$(Yi-Y)^2$
1	-3.51×10^{-4}	1.23×10^{-7}	-1.89×10^{-3}	3.57×10^{-6}	-1.51×10^{-3}	2.29×10^{-6}
20	-8.00×10^{-4}	6.40×10^{-7}	1.24×10^{-3}	1.54×10^{-6}	-4.33×10^{-5}	1.88×10^{-9}
40	-1.13×10^{-3}	1.28×10^{-6}	-2.39×10^{-3}	5.70×10^{-6}	1.58×10^{-3}	2.49×10^{-6}
60	2.40×10^{-3}	5.77×10^{-6}	5.23×10^{-4}	2.73×10^{-7}	1.19×10^{-3}	1.41×10^{-6}
80	-9.19×10^{-4}	8.44×10^{-7}	-8.63×10^{-4}	7.44×10^{-7}	-3.85×10^{-4}	1.48×10^{-7}
100	-5.71×10^{-4}	3.26×10^{-7}	-8.68×10^{-5}	7.54×10^{-9}	1.73×10^{-3}	2.98×10^{-6}
120	1.51×10^{-3}	2.29×10^{-6}	-1.61×10^{-3}	2.59×10^{-6}	-1.23×10^{-3}	1.53×10^{-6}
140	-5.11×10^{-5}	2.61×10^{-9}	-1.16×10^{-3}	1.35×10^{-6}	7.31×10^{-4}	5.35×10^{-7}
160	-1.55×10^{-3}	2.40×10^{-6}	-8.38×10^{-4}	7.02×10^{-7}	9.54×10^{-4}	9.10×10^{-7}
180	1.01×10^{-3}	1.03×10^{-6}	-3.40×10^{-4}	1.15×10^{-7}	-4.31×10^{-4}	1.86×10^{-7}
200	-3.37×10^{-4}	1.13×10^{-7}	-1.21×10^{-3}	1.46×10^{-6}	1.42×10^{-3}	2.01×10^{-6}
V_x^2	1.48×10^{-5}		1.81×10^{-5}		1.45×10^{-5}	
RMS	1.22×10^{-3}		1.34×10^{-3}		1.20×10^{-3}	
LOD (ppb)	6.89×10^{-2}		7.60×10^{-2}		6.81×10^{-2}	

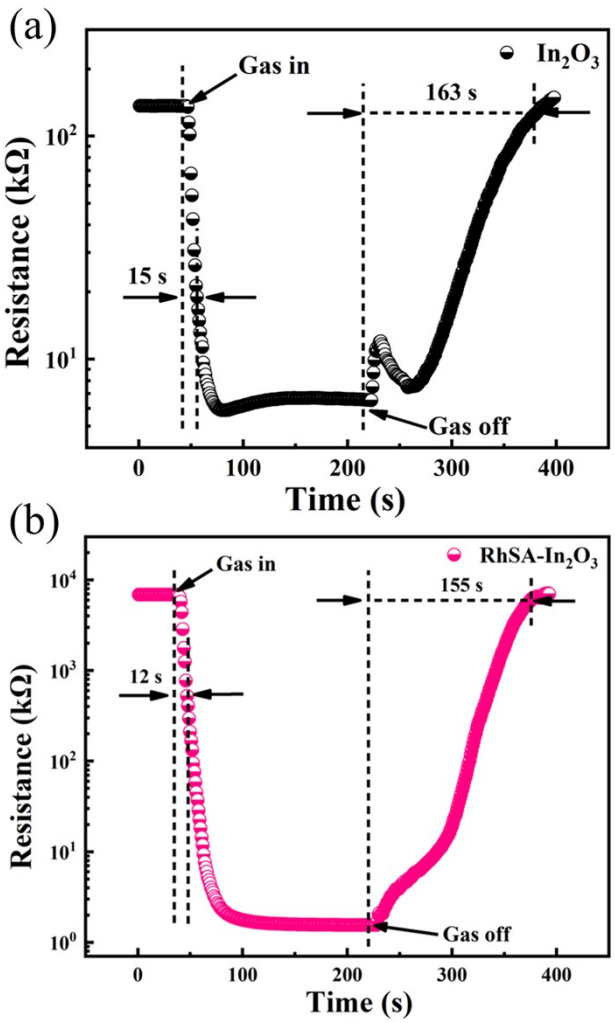

Fig. S8 Response and recovery curves of the In_2O_3 and RhSA-In_2O_3 sensors to 50 ppm ethanol at the working temperature of 260°C.

Table S4 Vibrational mode assignments of the surface species.

Species	Vibration mode	Location	Ref.
-OH	V_{-OH}	3000-3900 cm^{-1}	11
	δ_{H-O-H}	～1610 cm^{-1}	12
$-CH_3-$	V_{C-H}	2950 cm^{-1}	13
	δ_{C-H}	～1478 cm^{-1}	13
CO_2	$V_{O=C=O}$	2280-2390 cm^{-1}	14
CH_3CHO	$V_{C=O}$	1715 cm^{-1}	15
	V_{C-H}	2780 cm^{-1}	16
Acetic acid	V_{C-O}	1280 cm^{-1}	17

To verify the effect of adsorbed oxygen, a control experiment was carried out under Ar conditions. As shown in Fig. S9, the response of RhSA-In_2O_3 and In_2O_3 was 4590.32±127.07 and 52.51±2.82 in Air, while the response of RhSA-In_2O_3 and In_2O_3 was 8.353±0.56 and 2.88±0.11 in Ar, demonstrating that the presence of adsorbed oxygen is essential for the gas-sensitive response.

The role played by adsorbed oxygen in sensing reactions is mainly to carry out surface redox reactions with the measured gas. The high adsorbed oxygen content promoted the redox reaction and thus resulted in the good sensing performance.

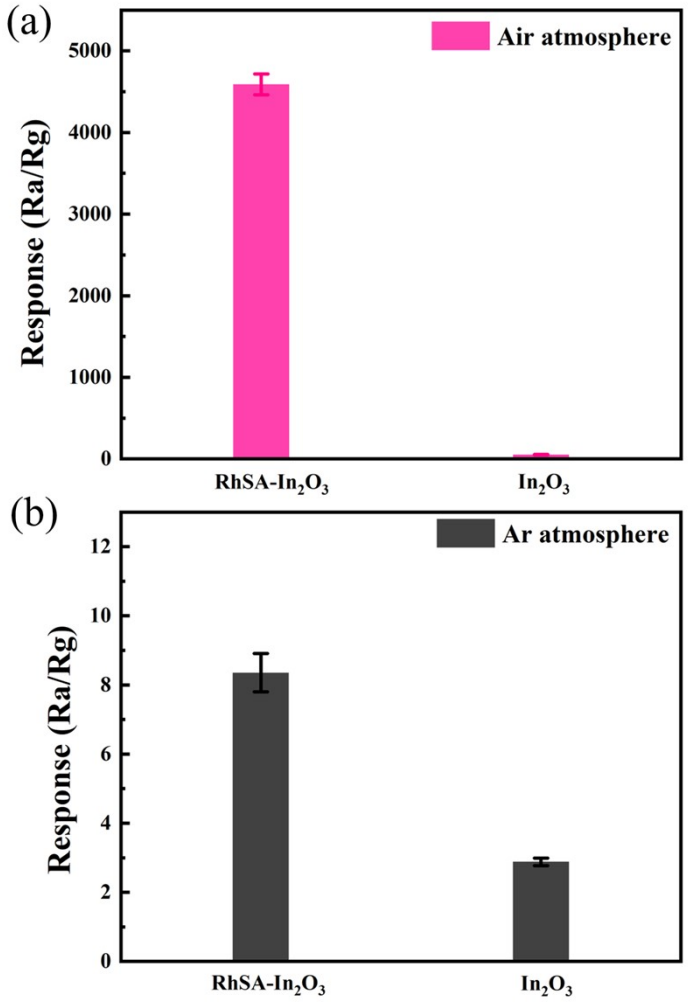

Fig. S9 The response of RhSA-In_2O_3 sensor to 50 ppm ethanol in Air (a) and in Ar (b) atmosphere.

References

1 Z. Dong, Q. Hu, H. Liu, Y. Wu, Z. Ma, Y. Fan, R. Li, J. Xu and X. Wang, *Sens. Actuators, B,* 2022, **357**, 131227.

2 Z. Cao, W. Wang, H. Ma, L. Xiao, J. Li, Y. Sun, J. Sheng and F. Dong, *Sens. Actuators, B,* 2022, **353**,131155.

3 L. Cai, X. Dong, G. Wu, J. Sun, N. Chen, H. Wei, S. Zhu, Q. Tian, X. Wang, Q. Jing, P. Li and B. Liu, *Sensors and Actuators, B*, 2022, **351**, 130863.

4 T. Liu, T. Wang, H. Li, J. Su, X. Hao, F. Liu, F. Liu and X. Liang, *Sensors and Actuators, B*, 2021, **349**, 130771.

5 P. Cao, Z. Yang, S. T. Navale, S. Han, S. Liu, W. Liu, Y. Lu, F. J. Stadler and D. Zhu, *Sensors and Actuators, B*, 2019, **298**, 126850.

6 F. Zhang, X. Li, Q. Zhao, G. Chen and Q. Zhang, *Appl. Catal. B,* 2020, **263**, 118278.

7 T. Y. Su, Y. Z. Chen, Y. C. Wang, S. Y. Tang, Y. C. Shih, F. Cheng, Z. M. Wang, H. N. Lin and Y. L. Chueh, *J. Mater. Chem. C*, 2020, **8**, 4851-4858.

8 Y. Song, F. Gu, Z. Wang and D. Han, *ACS Appl. Nano Mater.*, 2022, **5**, 15298-15309.

9 W. Liu, D. Gu and X. Li, *ACS Appl. Mater. Interfaces*, 2021, **13**, 20336-20348.

10 Z. Wu, L. Rong, J. Yang, Y. Wei, K. Tao, Y. Zhou, B. R. Yang, X. Xie and J. Wu, *Small,* 2021, **17**, 2104997.

11 M. M. Soraya, F. B. M. Ahmed and M. M. Mahasen, *J Mater Sci: Mater Electron*, 2022, **33**, 22077-22091.

12 C. V. S. Almeida, D. S. Ferreira, H. Huang, A. C. Gaiotti, G. A. Camara, A. E. Russell, K. I. B. Eguiluz and G. R. Salazar-Banda, *Appl. Catal. B*, 2019, **254**, 113-127.

13 V. V. Kaichev, Y. A. Chesalov, A. A. Saraev, A. Y. Klyushin, A. Knop-Gericke, T. V. Andrushkevich and V. I. Bukhtiyarov, *J Catal.,* 2016, **338**, 82-93.

14 Z. Mu, S. Chen, Y. Wang, Z. Zhang, Z. Li, B. Xin and L. Jing, *Small Sci.,* 2021, **1**, 2100050.

15 M. Roca-Ayats, O. Guillén-Villafuerte, G. García, M. Soler-Vicedo, E. Pastor and M. V. Martínez-Huerta, *Appl. Catal. B,* 2018, **237**, 382-391.

16 V. Rimal, S. Shishodia and P. K. Srivastava, *Appl. Nanosci.,* 2020, **10**, 455-464.

17 K. Liu, W. Wang, P. Guo, J. Ye, Y. Wang, P. Li, Z. Lyu, Y. Geng, M. Liu and S. Xie, *Adv. Funct. Mater*. 2018, **29**, 1806300.